Original Article

A Finite Element Study of Ultrasound Elastography Using Shear Wave Interference Patterns Generated by Miniature Surface Sources

Pezhman Pasyar[1], Vahid Sadeghi[1], Hassan Rezazadeh[1], Milad Askari[2], Alireza Mirbagheri[3], Seyed M Alavian[4], Hossein Arabalibeik[3]

1- Department of Medical Physics and Biomedical Engineering, Tehran University of Medical Sciences, Tehran, Iran.

2- Department of Mechanical Engineering, Tehran University, Tehran, Iran.

3- Research Center of Biomedical Technology and Robotics (RCBTR), Tehran University of Medical Sciences, Tehran, Iran.

4- Research Center for Gastroenterology and Liver Disease, Baqiyatallah University of Medical Sciences, Tehran, Iran.

Received: 19 March 2017

Accepted: 14 May 2017

Key Words:
Cross Correlation,
Elastic Waves,
Finite Element Analysis,
Interference Patterns,
Liver Elastography,
Mechanical Stimulation,
Ultrasound Imaging.

ABSTRACT

Purpose- Elastography as one of the most promising non-invasive methods in the diagnosis of liver diseases is attracting much attention. An interesting technique which is independent of imaging rate uses shear wave interference patterns induced by two external stimulation sources.

Methods- In this article a 3D finite element model of liver tissue with superficial mechanical stimulation is presented through which the possibility of using shear wave interference patterns to determine the type of liver fibrosis is investigated. In addition, the effect of various stimulation characteristics on the propagation of elastic waves and formation of shear wave interference patterns can be measured. Besides, ultrasound imaging and methods based on cross correlation are used to find target displacements caused by interference of shear waves.

Result and Discussion- Since the goal of this essay is to find the type of fibrosis, the results show achieving a high correlation between real and estimated elasticities (Pearson's coefficient of 0.9953 and P-value <0.05). Herein, the mean elasticity estimation for the stages of mild, sign, severe, and cirrhosis obtained respectively, is as follows: 4.79±1.5, 8.01±0.7, 11.3±2, and 31.21±16 kPa.

1. Introduction

Histological studies show that changes in microscopic structure of soft tissues, such as the emergence of cancerous tumors, can change the tissue stiffness or elasticity. In some diseases, like breast or prostate cancer, there are differences between the stiffness of cancerous areas and other normal areas [1]. This fact is in harmony with the ancient routine of manual palpation which has been used to apply pressure on soft tissues and find their abnormal conditions. Based on previous research, there have always been restrictions such as inaccessibility to some organs and the lack of contrast between lesions and normal tissues in such qualitative methods [2]. Moreover, in liver as the largest gland in the body, fibrosis causes stiffness variation throughout the tissue. In response to chronic liver injuries and diseases (such as hepatitis), collagenous fibrils replace the liver cells and the tissue stiffness

**Corresponding Author*:
Hossein Arabalibeik, PhD
Research Center of Biomedical Technology and Robotics (RCBTR), Tehran University of Medical Sciences, Tehran, Iran.
Tel: (+98)2166581505 / Fax: (+98)2166581533.
Email: arabalibeik@tums.ac.ir

increases. Advanced fibrosis (cirrhosis) eventually leads to liver failure, and cirrhosis is also associated with liver cancer. Studies show that the probability of liver cancer in patients with cirrhosis increases approximately by 5% per year. So a frequent non-invasive monitoring of liver stiffness could prevent many cancers and transplantations [3].

The primary studies about elastography techniques were conducted nearly two decades ago. Non-invasive elastography techniques could be classified according to the imaging method. The most common imaging methods in elastography are magnetic resonance [4-6] and ultrasound [7-34] imaging.

In this essay, we consider the ultrasound-based elastography, which has some advantages such as mobility and real time capability over the other imaging modalities. Most of the studies are focused on the ultrasound technique since it is more accessible, inexpensive, safe and comfortable [22, 27].

This technique can be divided into four categories depending on the type of external stimuli: compressional elastography [14, 17], transient vibrational elastography [18, 21, 24, 30, 34], continuous vibrational elastography [8, 9, 11, 13, 15, 25-29, 32, 33] and acoustic radiation force elastography [5, 12, 16, 19, 20, 31, 35].

A new method uses interference patterns of shear waves induced by two identical vibrating stimulation sources. The generated patterns, called standing waves, could be captured with a low frame rate ultrasound imaging system.

A superficial vibrating stress could be used to obtain the mechanical properties of target tissue by measuring its response to this stress. The other adjacent tissues in the path of stress induction and parameters of the vibrating source have effects upon the pattern formation and hence on the measured properties.

Wu *et al.* [25, 26] used sonoelastography for imaging interference patterns of shear waves. Sonoelastography is a method based on Doppler variance of the ultrasound echoes, which measures and images the amplitude of particle motions. In Wu's method, two vibrating sources were in contact with two sides of the medium and oscillated in parallel with these sides. The ultrasound transducer also was located in the path of vibrations. Then, images of interference patterns were analyzed to determine the elastic characteristics of the medium. This method had good results in ex vivo tests, but it was not appropriate for clinical applications due to the position and size of stimulation sources.

Hoyt *et al.* [28, 29] proposed the stimulation sources located perpendicular to the surface of the medium. They used developed algorithms to analyze images of interference patterns and to find viscoelastic characteristics of some tissues such as skeletal muscles. However, this method has disadvantages such as invalidity in some regions which lack planar propagation and for large diameters of stimulating shafts, which made it unsuitable for clinical use.

Partin *et al.* [33] used two small superficial stimulation sources which were perpendicular to the surface of tissue phantoms. However, their simulation of vibration field was valid only for point sources.

Palmeri *et al.* published their research as a guideline using finite element analysis for shear wave based elastography. In their study, three stages of the simulation of stress, applying stress, and the extraction of displacements data for other post-processing were explained. Nonetheless, these simulations are implemented for simple geometries and boundary conditions [36].

The 3D model presented in this study can be used to investigate any kind of elastography methods such as compression, transient, continuous, and acoustic radiation force and aid researchers in academic and industrial fields to reduce their experimental costs. Because our major goal is the liver fibrosis diagnosis, a continuous mechanical vibration is used for inducing shear wave interference patterns.

First, an approximate analytical closed form solution of the vibration field is discussed. Then, the FE model of a tissue phantom with two superficial mechanical stimulation sources, ultrasound imaging and methods for extracting interference patterns of shear waves and the results

are posed subsequently. Some discussions on the results and concluding remarks are provided in Sections 4 and 5 respectively.

2. Materials and Methods

2.1. Basic Theory

2.1.1. Mechanical Properties and Elastic Waves

Stress is the pressure due to applied load, which could appear in the form of tension, compression, shear, torsion, or their combination [37].

$$\sigma = \frac{F}{A_0} \quad (1)$$

Where F is the force and A_0 is the original cross sectional area. The response of the material to stress, i.e. the physical deformation (such as elongation) due to tension is called strain [37].

$$\varepsilon = \frac{L_i - L_0}{L_0} = \frac{\Delta L}{L_0} \quad (2)$$

Where L_i is instantaneous length and L_0 is the original length of material.

Elastic refers to a reversible non-permanent deformation where the material completely recovers to its original state upon release of the applied stress. According to the Hooke's law, in the linear isotropic elastic medium, the relationship between modulus of elasticity E (also known as Young's modulus), stress σ and strain ε is as follows [37]:

$$\sigma = E\varepsilon \quad (3)$$

Also if the strain along three dimensions is considered, the Poisson ratio v, shows the proportion of these directional strains [37],

$$v = -\frac{\varepsilon_x}{\varepsilon_z} = -\frac{\varepsilon_y}{\varepsilon_z} \quad (4)$$

Where ε_x, ε_y and ε_z are strains in x, y and z directions respectively. This ratio is approximately between 0.45 and 0.49 in soft tissues [39].

When a stress is applied to a solid body, the particles will be disturbed and transmit the energy to other parts of the body while returning to their equilibrium. These transmissions emerge as a wave propagation with a certain velocity. Elastic stress waves are divided into two parts, the body wave, and the surface wave. The body waves include longitudinal (or compressional) and transverse (or shear) waves. The surface wave is known as Rayleigh wave [40].

The fastest wave is the longitudinal body wave in which the direction of the particle motion is along the direction of wave propagation and can propagate in all mediums (solids, liquids and gases). Shear waves propagate perpendicular to the direction of particle motion and are slower than longitudinal waves and can only move through solids, not through any liquid or gas.

The Rayleigh wave which forms when the body has free surfaces, is slower than the shear wave, but has larger amplitude. The particles move in elliptical paths; however, as the depth into the solid increases, the width of the elliptical path decreases rapidly [40].

These waves propagate in the elastic body when a sudden disorder, like an impact, is applied to a point of it. Each wave has a certain propagation velocity. The propagation velocity of longitudinal wave c_L ,transverse wave c_T and Rayleigh wave c_R for a density ρ, are obtained from the following Equations respectively [40, 41].

$$c_L = \sqrt{\frac{E(1-v)}{\rho(1+v)(1-2v)}} \quad (5)$$

$$c_T = \sqrt{\frac{E}{2\rho(1+v)}} \quad (6)$$

$$c_R = c_T \frac{0.862+1.14v}{1+v} \quad (7)$$

As shown in Figure 1 the longitudinal and transverse waves propagate with a spherical wave front and the Rayleigh wave passes through the surface. Numbers indicate the relative velocity of each wave compared to longitudinal wave.

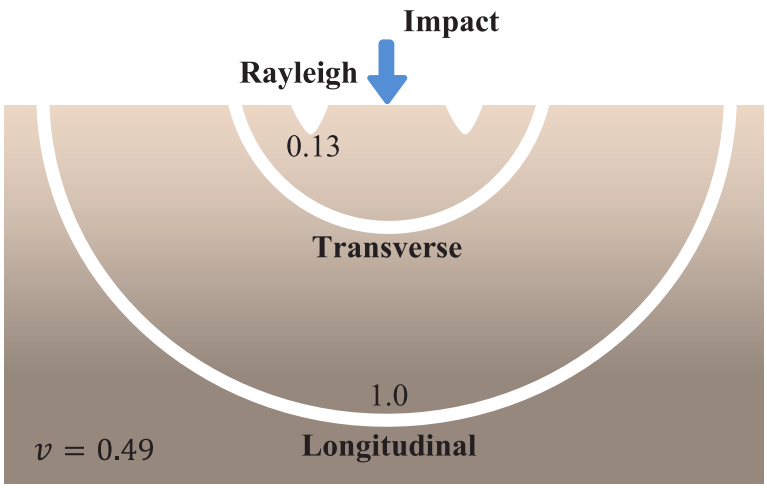

Figure 1. Elastic waves induced by an impact applied to a surface point [41]. The relative velocity of each wave compared to longitudinal wave for a Poisson ratio of 0.49 is also depicted.

2.12. Shear Wave Generated by Superficial Mechanical Stimulation

To investigate the vibration field caused by a circular disk vibrating normal to the surface of medium, Miller and Pursey [42] presented an analytical closed form solution. According to their proposed solution, the axial displacement of tissue particles in the far field and for a small vibrating source (R >> a), is:

$$u_z \sim \frac{ia^2\cos\theta}{2c_{44}R}\left(\frac{2\mu^3\sin^2\theta\sqrt{\mu^2\sin^2\theta-1}}{F_0(\mu\sin\theta)}e^{-i\mu R}+\frac{i\cos\theta(\mu^2-2\sin^2\theta)}{F_0(\sin\theta)}e^{-iR}\right)e^{i\omega t} \quad (8)$$

where $i=\sqrt{-1}$, a is the radius of circular disk vibrating normal to the surface, c_{44} is shear modulus, R is the distance from the vibrating source, μ is the ratio of $\frac{k_s}{k_c}$ with k_s and k_c being the shear wave number and the compressional wave number respectively, θ is the angle from the axial direction and ω is the frequency of vibrating source as shown in Figure 2.

In Equation 8, $F_0(\xi)$ is a complex function, which is defined as follows, and can be displayed as a phasor:

$$F_0(\xi) = (2\xi^2-\mu^2)^2 - 4\xi^2\sqrt{(\xi^2-1)}\sqrt{(\xi^2-\mu^2)} \quad (9)$$

$$F_0(\xi) = |F_0(\xi)|\exp(i\gamma) \quad (10)$$

Where γ is:

$$\gamma = \tan^{-1}\left(\frac{\mathrm{Im}(F_0(\xi))}{\mathrm{Re}(F_0(\xi))}\right) \quad (11)$$

To simplify Equation 8, the effect of compressional wave component can be neglected because the compressional wave usually propagates with high speed and its wavelength is longer than body organs. By adding the attenuation coefficient α_s, the following Equation can be obtained:

$$u_Z = \frac{A}{r}e^{-\alpha_s R}e^{\left(i\left(\omega t-\mu R-\gamma+\frac{\pi}{2}\right)\right)} \quad (12)$$

$$A = \frac{a^2\cos\theta}{2c_{44}}\frac{2\mu^3\sin^2\theta\sqrt{\mu^2\sin^2\theta-1}}{|F_0(\mu\sin\theta)|} \quad (13)$$

The function $u_Z(R,\theta,t)$ describes the displacement of each tissue node as a function of time and its distance and departure angle from the vibrating source. Assuming the center of ultrasound probe as the origin of coordinates (0,0), two vibrating sources located at (d_1,0) and (d_2,0) respectively can interfere in each node to create an interference pattern of shear waves.

$$U_T(R,\theta,t) = \sum_{i=1}^{2} u_{zi}(R_i,\theta_i,t) \quad (14)$$

However, equations provided in this Section are only valid for vibration sources with a small footprint. Therefore, they cannot be used for the optimization of some parameters via simulation.

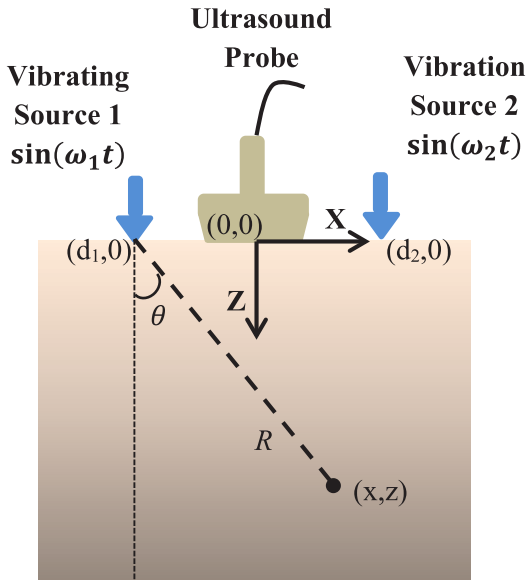

Figure 2. Schematic of the location of the ultrasound probe and sinusoidal vibrating sources in XZ plane which is in the direction of ultrasound beams. The center of the ultrasound transducer is regarded as the origin of coordinates and sources are located at distances d_1 and d_2 respectively.

2.1.3. Interference Patterns

Some previous studies have shown that the shear wave interference patterns can be used in ultrasound elastography [25, 26, 29]. In fact, shear wavelength λ, measured using patterns, is multiplied by frequency f to obtain wave speed, which is related to Young's modulus as depicted in Equation 6.

$$c_T = f\lambda \quad (15)$$

2.2. Simulation

2.2.1. Finite Element Model of Liver Tissue with Superficial Mechanical Stimulation

To generate and simulate the FE model, Abaqus FEA (Abaqus, Dassault Systems, France), which has an extensive range of material models such as elastomeric materials, was used. Herein a 15×15×15 cm^3 cubic model was meshed and analyzed while stimulated by two circular bars vibrating normal to the surface, with a given frequency, amplitude, separation distance, and shaft diameter as stimulation parameters. This model consists of several layers such as a superficial layer as the skin and fat; the second layer as the muscles between ribs; the chest ribs and the liver as the final layer.

Triangular elements with an approximation global size of about 1-4 mm were used to create the mesh. In order to capture the propagation wave at least 8-10 elements per wavelength is needed. Besdies, time increment step size should be small enough [43, 44]. Typically 20 points per cycle of the highest frequency is reasonable. We assumed a linear elastic material with isotropic behavior, Young modulus of 5 kPa and the density of 1059.9 kg/m^3 for skin and fat, and Young modulus of 7 kPa and density of 909.4 kg/m^3 for the muscle. Also, the ribs were defined as a rigid body and the Poisson ratio of 0.499 (as an incompressible material) was assigned to all tissues in the model. Finally, the Young modulus of liver with the density of 1000 kg/m^3 is changed from a healthy tissue to cirrhosis [39]. The boundary conditions are assumed to be reflected by free sliding of lateral faces and a fixed lower face of the cubic phantom. The FE model is illustrated in Figure 3.

FE analysis was performed on a machine with Intel Core-i7-2670QM and 8 gigabytes installed memory (RAM) running 64-bit Microsoft Windows 7.

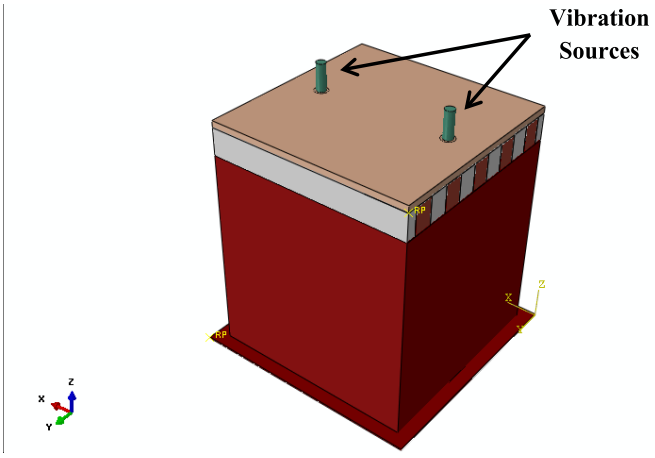

Figure 3. View of FE phantom used for the prediction of tissue displacements resulted from a stimulation by two circular bars, vibrating normal to the phantom surface, given predefined boundary conditions.

2.2.2. Ultrasound Imaging Simulation

To simulate the acoustic response of tissue model and ultrasound imaging, we have used Field II toolbox [45, 46]. Field II outputs are radio-frequency RF signals received from point scatters within the simulated phantom. Therefore, by applying beam forming methods, the B-mode image of the tissue could be simulated. In this study, an ultrasound imaging with a 128-element linear array transducer was simulated. Characteristics of the simulated transducer in Field II are listed in Table 1.

Table 1. Simulated transducer parameters.

Variable Name	Symbol	Value
Number of Elements	N	128
Active Elements	N_A	32
Transducer Center Frequency	F_C	5 MHz
Kerf	$kerf$	0.025 mm
Pitch	P	0.3048 mm
Sampling Rate	f_S	100 MHz
Focal Point	F	0.05 m

2.2.3. Extraction of Shear Wave Interference Patterns

Elastography includes applying a stress to the medium and estimating the resulting strain. To achieve this, RF data is obtained before and after applying stress. Then, the mechanical strain could be computed using speckle tracking or phase tracking methods. The resulting strain image is called elastogram. Generally speaking, cross-correlation based methods, applied to the amplitude or phase of the received RF data, could be considered as conventional methods in elastography [47]. Other methods such as Doppler imaging or using signal power "spectrum", compute the strain directly [8-10, 13].

To reveal shear wave interference patterns, we have used a cross-correlation method for detecting the displacement in the associated direction. According to this method, first the beam-formed RF signals related to consecutive frames during shear wave propagation were collected, and then the phase differences due to the movement of scatters were detected in these images. To achieve this, 2-D normalized cross-correlation were calculated from a series of consecutive images to track subsample movements. For this algorithm the following general procedure was used.

1. Select an image as the base and other images which have to be correlated as input.
2. Create grids of control points for the base and first input image.
3. Extract an 11-by-11 template around the input control point and a 21-by-21 region around the base control point.
4. Calculate the normalized cross-correlation of the template with the region.
5. Find the absolute peak of the cross-correlation matrix.
6. Use the position of the peak to adjust the coordinates of the input control point.
7. Update the input control point to adjusted coordinates from previous steps for the next input image and go to step 3.

All calculations were conducted using MATLAB (The Mathworks Inc., Natick, USA) software.

3. Results

After FE simulation, displacements of mesh nodes are transferred to MATLAB, where interpolation is used to find the displacement of every arbitrary non-mesh node. Figure 4 shows the results of inducing patterns in the simulated phantom for frequency of 50 Hz. The stimulation amplitude, stimulating shaft diameter and the distance between sources are considered to be 1 mm, 5 mm and 10 cm respectively.

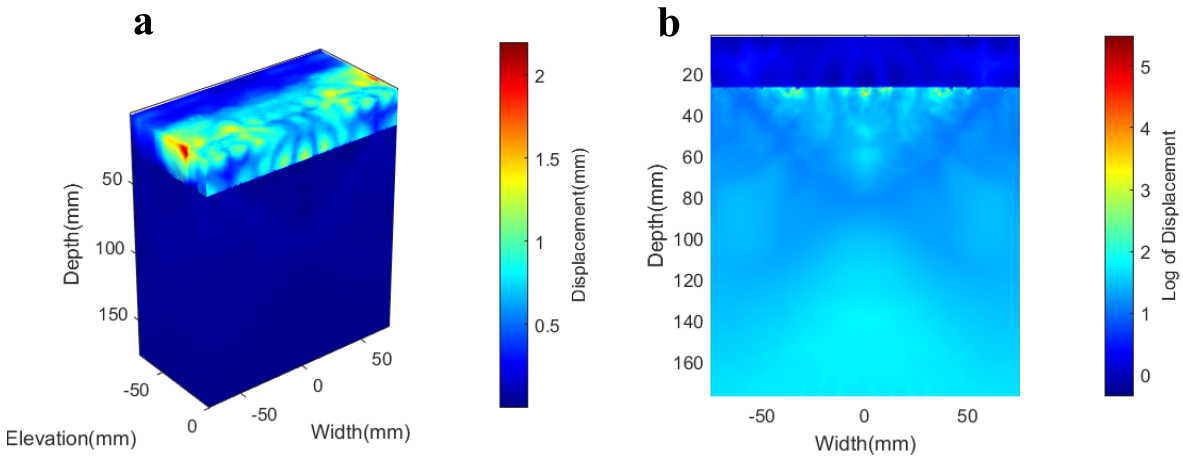

Figure 4. Shear wave interference patterns formation in the FE simulation. (a) Cross section of the cubic phantom. (b) The logarithmic representation of the patterns displacement formed in the vertical plane passing through 50 Hz sources.

Using the estimated displacements, B-mode ultrasound images of pre and post-stress phantoms are obtained by Field II toolbox which are then used in pattern extraction algorithm. Figure 5 shows an example of simulated B-mode ultrasound images and their related extracted patterns and shear speed map obtained from the Equation (15). Here, the gentle changes of wavelength and shear speed is compensated and assigned to the homogeneous phantom, by averaging the image of interference patterns in the axial direction. The average displacement which is fitted with a sinusoidal signal is depicted in figure 5d. Figure 5e shows the speed map obtained from the wavelength of sinusoidal signal. Here according to the phantom characteristics and 50 Hz sources, the shear wave speed should be equal to 1 m/s in the liver tissue.

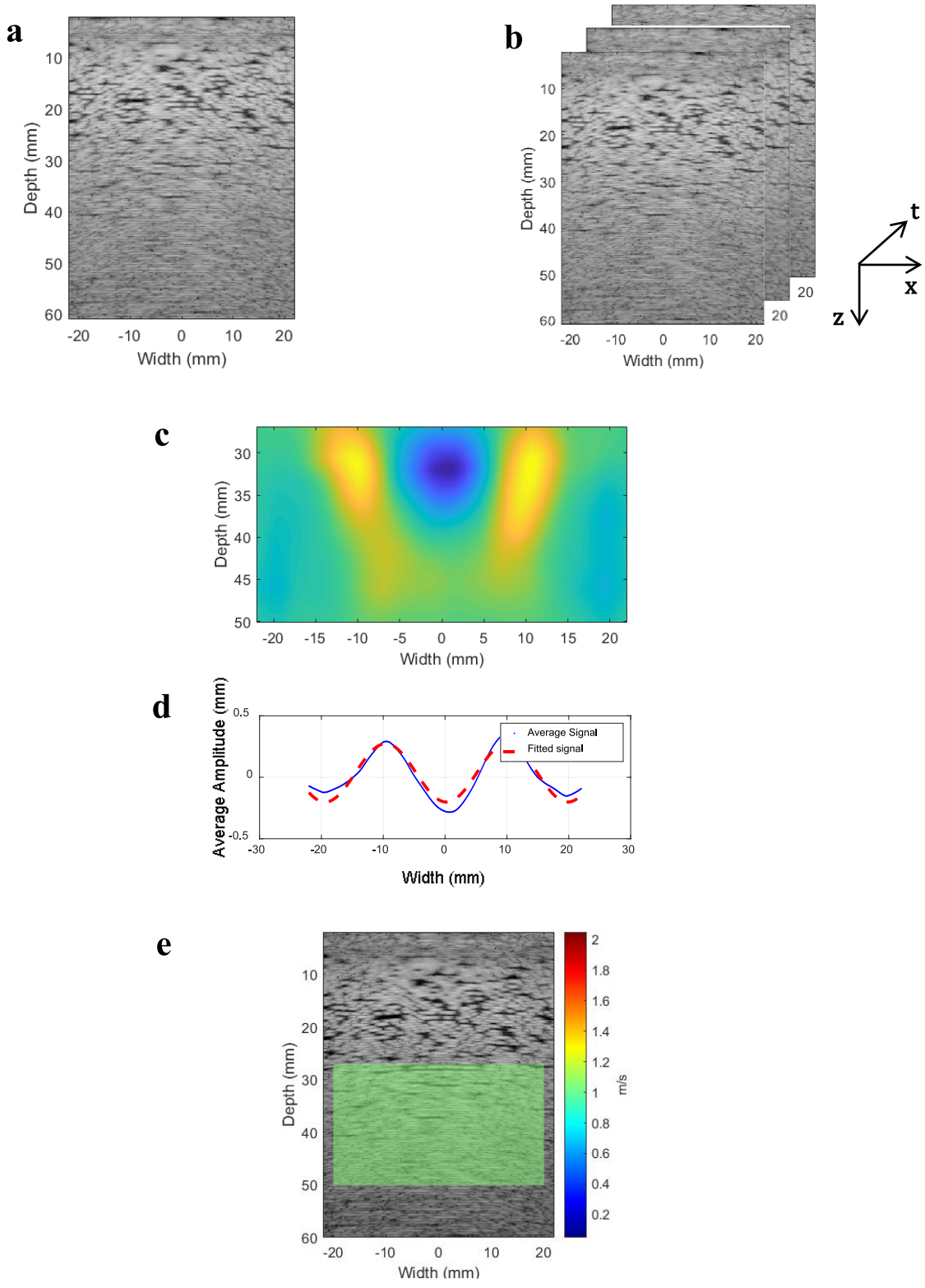

Figure 5. Extracting the interference patterns of shear waves. (a) B-mode ultrasound images before applying the stress (the base image); (b) Series of consecutive images during shear wave propagation (c) Extracted patterns; (d) Average displacement and fitted sinusoidal signals; (e) Shear speed map of the phantom.

3.1. Algorithm Evaluation

The elasticity of phantoms with different stiffnesses are calculated using the proposed algorithm and the estimated elasticity is obtained vs. true elasticity and shown in Table 2. The range of stiffness used is changed from mild liver fibrosis to cirrhosis [48, 49].

Table 2. Elasticity estimation errors for different ranges of stiffness in chronic liver diseases.

	Fibrosis							
	Mild		Sign		Severe		Cirrhosis	
	True Elasticity (kPa)	Estimated Elasticity (kPa)	True Elasticity (kPa)	Estimated Elasticity (kPa)	True Elasticity (kPa)	Estimated Elasticity (kPa)	True Elasticity (kPa)	Estimated Elasticity (kPa)
	3	3.24	7	6.98	9.5	8.94	12.5	14.12
	4	3.66	7.5	7.97	10	9.61	20	20.71
	5	4.57	8	8.56	11	11.49	30	27
	6	5.53	8.5	7.64	12	12.38	40	40.04
	7	6.98	9.5	8.94	12.5	14.12	50	54.18
Mean (kPa)	5	4.79	8.1	8.01	11	11.3	30.5	31.21

As shown in Table 3, mean real phantom's elasticity for 20 cases is 13.65 ± 12.37 kPa, while for the proposed algorithm is 13.83 ± 12.92 kPa. To evaluate the parity between these two sets of data, the Pearson's coefficient is computed.

Table 3. Pearson's correlation between two sets of real and estimated data.

		Mean	STD	Pearson's Coefficient	P-value
Technique	True Elasticity (kPa)	13.65	12.37	0.9953	<0.05
	Algorithm (kPa)	13.83	12.92		

4. Discussion

The 3D model presented in this study can be used to investigate any kind of elastography methods such as compression, transient, continuous, and acoustic radiation force and aid researchers in academic and industrial fields to reduce their experimental costs. However, since our major goal is liver fibrosis diagnosis, a continuous mechanical vibration for inducing shear wave interference patterns was presented.

Elastography using shear waves interference patterns could be considered as a non-invasive remote palpation with widespread applications in the diagnosis of diseases that change the stiffness of tissue. Also to reveal patterns, a normalized cross correlation based method was applied to the ultrasound images. As a result, subsample displacements could be extracted.

Wu *et al.* [25, 26] used two vibrating sources on the opposite sides of the medium generating a sliding movement. It was not appropriate for clinical applications due to the position and size of stimulation sources. Hoyt *et al.* [28, 29] used rectangular bars vibrated perpendicular to the surface of the medium which made it unsuitable for clinical use. Partin *et al.* [33] used two small superficial stimulation sources perpendicular to the surface of tissue phantoms. However, their simulation is valid only for point sources.

The shear wave velocity estimation errors in Wu's method for the experimental low and high stiffness phantoms were under 4% and 2% respectively [25,

26]. In addition, the average shear wave speed estimation error for the Hoyt's simulation-based sonoelastogram and experimental homogeneous phantom were obtained 2.3% and 4.4% [28, 29]. The error in the Partin's method was 4.5% for a homogeneous phantom [33]. Despite these acceptable results, the mentioned works had some disadvantages in clinical usage and in their simulations which could not observe effective parameters in the elastography process. In this article, by proposing the miniature surface sources and accompanying it with the finite element analysis, these defects were covered. Also the possibility of using the interference of shear waves for many organs has not been investigated yet for elastography. So this numerical study conducted to prove the ability of this method for the liver tissue, exclusively.

We also considered the set of elastic waves, the longitudinal, transverse and Rayleigh surface waves in order to evaluate their effects on shear wave interference patterns and regenerate the real conditions more accurately. Interference patterns of shear waves in Figure 4 reveal that the wavelength decreases with increasing stimulation frequency. Therefore, the frequency should be opted in such a way that several wavelengths of patterns could be formed between sources.

In Figure 5, some simulated ultrasound images with their extracted patterns are shown. The blue and red colors in Figure 5c indicate the particles' motion toward and away from the ultrasound transducer respectively. The borders between these two colors represent the fixed points of the patterns. Figure 5e illustrates the shear speed map, obtained from the wavelength of patterns using Equation (15). According to these results, when the depth increases, the patterns' wavelength changes slightly. We compensate this, by averaging the image of interference patterns in the axial direction. Finally, the average displacement which is fitted with a sinusoidal signal is used to obtain the shear speed map and assign to the homogeneous phantom.

The proposed method estimates the tissue elasticity by measuring the wavelength of shear wave interference patterns. Therefore, the accuracy in determining the wavelength is one of the most influential factors in determining the accuracy of elastography. In fact, the error in the determination of tissue elasticity is the square root of the error occurred in the wavelength measurement.

As shown in Table 2, the elasticity was estimated for each stage of fibrosis with the proposed algorithm and compared with the real phantom's elasticity. This procedure was repeated for five different stiffness at each stage (from mild liver fibrosis to cirrhosis). Since the goal of this essay is to find the type of fibrosis, the results show achieving a high correlation between the real and estimated elasticities (Pearson's coefficient of 0.9953 and P-value<0.05). Herein, the mean elasticity estimation for the stages of mild, sign, severe, and cirrhosis obtained respectively, is as follows: 4.79±1.5 kPa, 8.01±0.7 kPa, 11.3±2 kPa, and 31.21±16 kPa. It is expected that our proposed solution as a frequent non-invasive monitoring of liver stiffness could prevent many liver cancers and transplantations.

5. Conclusion

The purpose of elasticity imaging, commonly known as elastography, is to estimate the mechanical properties of a medium from the distributed strain caused by a stress field. Dynamic elastography methods that use the vibration surface sources have several advantages, such as non-invasiveness and low cost. A method for generating low-frequency shear waves in soft tissue is investigated by using the mechanical surface force resulting from two intersecting oscillating sources that vibrate vertically on the surface. Also, the generated patterns are extracted by measuring the displacement of tissue particles through applying a correlation based method to the images acquired during the propagation of shear waves. Given the shear wave interference pattern, the shear wave velocity and elasticity of liver could be obtained.

A finite element model of tissue with superficial mechanical stimulation is presented. Using this model, the effects of various effecting parameters on the propagation of elastic waves, formation of interference patterns and elasticity estimation error can be measured. Our findings suggest that the proposed method can be used for the diagnosis of liver fibrosis level and prevent many cancers and transplantations as a continuous non-invasive monitoring.

Acknowledgments

This research has been supported by Tehran University of Medical Sciences & Health Services grant 94-04-30-30918.

References

1- W. Anderson, "Pathology (8'th ed.)," *Saint Louis, Mo, USA: CW Mosby Co,* 1984.

2- D. C. Wolf, "Evaluation of the size, shape, and consistency of the liver," 1990.

3- E. L. Carstensen, K. J. Parker, and R. M. Lerner, "Elastography in the management of liver disease," *Ultrasound in medicine & biology,* vol. 34, no. 10, pp. 1535-1546, 2008.

4- R. Muthupillai, D. Lomas, P. Rossman, J. Greenleaf, A. Manduca, and R. Ehman, "Magnetic resonance elastography by direct visualization of propagating acoustic strain waves," *Science,* vol. 269, no. 5232, pp. 1854-1857, 1995.

5- A. P. Sarvazyan, O. V. Rudenko, S. D. Swanson, J. B. Fowlkes, and S. Y. Emelianov, "Shear wave elasticity imaging: a new ultrasonic technology of medical diagnostics," *Ultrasound in medicine & biology,* vol. 24, no. 9, pp. 1419-1435, 1998.

6- J. Lorenzen, R. Sinkus, M. Biesterfeldt, and G. Adam, "Menstrual-cycle dependence of breast parenchyma elasticity: estimation with magnetic resonance elastography of breast tissue during the menstrual cycle," *Investigative radiology,* vol. 38, no. 4, pp. 236-240, 2003.

7- R. Dickinson and C. Hill, "Measurement of soft tissue motion using correlation between A-scans," *Ultrasound in medicine & biology,* vol. 8, no. 3, pp. 263-271, 1982.

8- T. Krouskop, D. Dougherty, and F. Vinson, "A pulsed Doppler ultrasonic system for making noninvasive measurements of the mechanical properties of soft tissue," *J Rehabil Res Dev,* vol. 24, no. 2, pp. 1-8, 1987.

9- R. M. Lerner, K. J. Parker, J. Holen, R. Gramiak, and R. C. Waag, "Sono-elasticity: medical elasticity images derived from ultrasound signals in mechanically vibrated targets," in *Acoustical imaging*: Springer, 1988, pp. 317-327.

10- S. R. Huang, R. M. Lerner, and K. J. Parker, "On estimating the amplitude of harmonic vibration from the Doppler spectrum of reflected signals," *The Journal of the Acoustical Society of America,* vol. 88, no. 6, pp. 2702-2712, 1990.

11- K. Parker, S. Huang, R. Musulin, and R. Lerner, "Tissue response to mechanical vibrations for "sonoelasticity imaging"," *Ultrasound in medicine & biology,* vol. 16, no. 3, pp. 241-246, 1990.

12- T. Sugimoto, S. Ueha, and K. Itoh, "Tissue hardness measurement using the radiation force of focused ultrasound," in *Ultrasonics Symposium, 1990. Proceedings., IEEE 1990*, 1990, pp. 1377-1380: IEEE.

13- Y. Yamakoshi, J. Sato, and T. Sato, "Ultrasonic imaging of internal vibration of soft tissue under forced vibration," *Ultrasonics, Ferroelectrics, and Frequency Control, IEEE Transactions on,* vol. 37, no. 2, pp. 45-53, 1990.

14- J. Ophir, I. Cespedes, H. Ponnekanti, Y. Yazdi, and X. Li, "Elastography: a quantitative method for imaging the elasticity of biological tissues," *Ultrasonic imaging,* vol. 13, no. 2, pp. 111-134, 1991.

15- L. Gao, K. Parker, S. Alam, and R. Lerner, "Sonoelasticity imaging: theory and experimental verification," *The Journal of the Acoustical Society of America,* vol. 97, no. 6, pp. 3875-3886, 1995.

16- M. Fatemi and J. F. Greenleaf, "Ultrasound-stimulated vibro-acoustic spectrography," *Science,* vol. 280, no. 5360, pp. 82-85, 1998.

17- T. A. Krouskop, T. M. Wheeler, F. Kallel, B. S. Garra, and T. Hall, "Elastic moduli of breast and prostate tissues under compression," *Ultrasonic imaging,* vol. 20, no. 4, pp. 260-274, 1998.

18- S. Catheline, F. Wu, and M. Fink, "A solution to diffraction biases in sonoelasticity: the acoustic impulse technique," *The Journal of the Acoustical Society of America,* vol. 105, no. 5, pp. 2941-2950, 1999.

19- K. R. Nightingale, R. W. Nightingale, M. L. Palmeri, and G. E. Trahey, "A finite element model of remote palpation of breast lesions using radiation force: Factors affecting tissue displacement," *Ultrasonic Imaging,* vol. 22, no. 1, pp. 35-54, 2000.

20- K. R. Nightingale, M. L. Palmeri, R. W. Nightingale, and G. E. Trahey, "On the feasibility of remote palpation using acoustic radiation force," *The Journal of the Acoustical Society of America,* vol. 110, no. 1, pp. 625-634, 2001.

21- L. Sandrin, M. Tanter, J.-L. Gennisson, S. Catheline, and M. Fink, "Shear elasticity probe for soft tissues with 1-D transient elastography," *Ultrasonics, Ferroelectrics, and Frequency Control, IEEE Transactions on,* vol. 49, no. 4, pp. 436-446, 2002.

22- J. F. Greenleaf, M. Fatemi, and M. Insana, "Selected methods for imaging elastic properties of biological tissues," *Annual review of biomedical engineering,* vol. 5, no. 1, pp. 57-78, 2003.

23- E. E. Konofagou and K. Hynynen, "Localized harmonic motion imaging: theory, simulations and experiments," *Ultrasound in medicine & biology,* vol. 29, no. 10, pp. 1405-1413, 2003.

24- J. Bercoff, M. Tanter, and M. Fink, "Supersonic shear imaging: a new technique for soft tissue elasticity mapping," *Ultrasonics, Ferroelectrics, and Frequency Control, IEEE Transactions on,* vol. 51, no. 4, pp. 396-409, 2004.

25- Z. Wu, L. S. Taylor, D. J. Rubens, and K. J. Parker, "Sonoelastographic imaging of interference patterns for estimation of the shear velocity of homogeneous biomaterials," *Physics in medicine and biology,* vol. 49, no. 6, p. 911, 2004.

26- Z. Wu, K. Hoyt, D. J. Rubens, and K. J. Parker, "Sonoelastographic imaging of interference patterns for estimation of shear velocity distribution in biomaterials," *The Journal of the Acoustical Society of America,* vol. 120, no. 1, pp. 535-545, 2006.

27- K. Hoyt, K. J. Parker, and D. J. Rubens, "Real-time shear velocity imaging using sonoelastographic techniques," *Ultrasound in medicine & biology,* vol. 33, no. 7, pp. 1086-1097, 2007.

28- K. Hoyt, B. Castaneda, and K. J. Parker, "Two-dimensional sonoelastographic shear velocity imaging," *Ultrasound in medicine & biology,* vol. 34, no. 2, pp. 276-288, 2008.

29- K. Hoyt, T. Kneezel, B. Castaneda, and K. J. Parker, "Quantitative sonoelastography for the in vivo assessment of skeletal muscle viscoelasticity," *Physics in medicine and biology,* vol. 53, no. 15, p. 4063, 2008.

30- R. Z. Azar, A. Baghani, S. E. Salcudean, and R. Rohling, "Dynamic elastography using delay compensated and angularly compounded high frame rate 2D motion vectors," in *Ultrasonics Symposium (IUS), 2010 IEEE*, 2010, pp. 1616-1619: IEEE.

31- K. Hoyt, Z. Hah, C. Hazard, and K. J. Parker, "Experimental validation of acoustic radiation force induced shear wave interference patterns," *Physics in medicine and biology,* vol. 57, no. 1, p. 21, 2011.

32- K. Lin, J. R. McLaughlin, A. Thomas, K. Parker, B. Castaneda, and D. J. Rubens, "Two-dimensional shear wave speed and crawling wave speed recoveries from in vitro prostate data," *The Journal of the Acoustical Society of America,* vol. 130, no. 1, pp. 585-598, 2011.

33- A. Partin, Z. Hah, C. T. Barry, D. J. Rubens, and K. J. Parker, "Elasticity estimates from images of crawling waves generated by miniature surface sources," *Ultrasound in medicine & biology,* vol. 40, no. 4, pp. 685-694, 2014.

34- A. J. Engel and G. R. Bashford, "A new method for shear wave speed estimation in shear wave elastography," *IEEE transactions on ultrasonics, ferroelectrics, and frequency control,* vol. 62, no. 12, pp. 2106-2114, 2015.

35- M. Soozande, H. Arabalibeik, And S. M. Alavian, "Reduced Imaging Rate in Liver Elastometery Using Shear Wave Interference Patterns," *Medicine Meets Virtual Reality 22: NextMed/MMVR22,* vol. 220, p. 390, 2016.

36- M. L. Palmeri, B. Qiang, S. Chen, and M. W. Urban, "Guidelines for Finite-Element Modeling of Acoustic Radiation Force-Induced Shear Wave Propagation in Tissue-Mimicking Media," *IEEE transactions on ultrasonics, ferroelectrics, and frequency control,* vol. 64, no. 1, pp. 78-92, 2017.

37- J. Wulff, *Structure and Properties of Materials: Mechanical behavior, by HW Hayden, LG Moffatt, and J. Wulff.* Wiley, 1965.

38- R. Mini, C. Krishnamurthy, K. Balasubramaniam1and, and P. Ravindran, "wave propagation through isotropic, linear elastic material using mass spring lattice model."

39- E. J. Chen, J. Novakofski, W. K. Jenkins, and W. D. O'Brien, "Young's modulus measurements of soft tissues with application to elasticity imaging," *IEEE Transactions on ultrasonics, ferroelectrics, and frequency control,* vol. 43, no. 1, pp. 191-194, 1996.

40- M. Tabatabaee Ghomi, "modelling and simulation of elastic & plastic behaviour of propagating impact wave: Impact-echo and Explosive welding process development," Mälardalen University, 2011.

41- M. Sansalone, "Impact-echo: the complete story," *ACI structural journal,* vol. 94, no. 6, pp. 777-786, 1997.

42- G. Miller and H. Pursey, "The field and radiation impedance of mechanical radiators on the free surface of a semi-infinite isotropic solid," in *Proceedings of the Royal Society of London A: Mathematical, Physical and Engineering Sciences*, 1954, vol. 223, no. 1155, pp. 521-541: The Royal Society.

43- M.-f. Zheng, C. Lu, G.-z. Chen, and P. Men, "Modeling three-dimensional ultrasonic guided wave propagation and scattering in circular cylindrical structures using finite element approach," *Physics Procedia,* vol. 22, pp. 112-118, 2011.

44- M. Hussin, T. H. Chan, S. Fawzia, and N. Ghasemi, "Finite element modelling of lamb wave propagation in prestress concrete and effect of the prestress force on the wave's characteristic," 2015.

45- J. A. Jensen and N. B. Svendsen, "Calculation of pressure fields from arbitrarily shaped, apodized, and excited ultrasound transducers," *IEEE transactions on ultrasonics, ferroelectrics, and frequency control,* vol. 39, no. 2, pp. 262-267, 1992.

46- J. A. Jensen, "Field: A program for simulating ultrasound systems," *In 10th nordicbaltic conference on biomedical imaging,* vol. 4, Supplement 1, part 1: 351--353, 1996: Citeseer.

47- K. Parker, M. Doyley, and D. Rubens, "Corrigendum: Imaging the elastic properties of tissue: the 20 year perspective," *Physics in Medicine and Biology,* vol. 57, no. 16, p. 5359, 2012.

48- L. Castera, X. Forns, and A. Alberti, "Non-invasive evaluation of liver fibrosis using transient elastography," *Journal of hepatology,* vol. 48, no. 5, pp. 835-847, 2008.

49- S. Mueller and L. Sandrin, "Liver stiffness: a novel parameter for the diagnosis of liver disease," *Hepat Med,* vol. 2, pp. 49-67, 2010.

50- R. K. Wang, Z. Ma, and S. J. Kirkpatrick, "Tissue Doppler optical coherence elastography for real time strain rate and strain mapping of soft tissue," *Applied Physics Letters,* vol. 89, no. 14, p. 144103, 2006.